Proceedings of the All-Polish Seminar on Mössbauer Spectroscopy, Goniądz, Poland, June 17–20, 2018

Structure and Hyperfine Interactions of Fe-Doped ZnO Powder Prepared by Co-Precipitation Method

J. Grotel[a], T. Pikula[b], K. Siedliska[b], L. Ruchomski[c], R. Panek[d], M. Wiertel[e] and E. Jartych[b,*]

[a]Lublin University of Technology, Faculty of Electrical Engineering and Computer Science, Nadbystrzycka 38A, 20-618 Lublin, Poland

[b]Lublin University of Technology, Institute of Electronics and Information Technology, Nadbystrzycka 38A, 20-618 Lublin, Poland

[c]Lublin University of Technology, Institute of Electrical Engineering and Electrotechnologies, Nadbystrzycka 38A, 20-618 Lublin, Poland

[d]Lublin University of Technology, Department of Geotechnics, Nadbystrzycka 40, 20-618 Lublin, Poland

[e]Institute of Physics, University of Maria Curie-Skłodowska, pl. M. Curie-Skłodowskiej 1, 20-031 Lublin, Poland

In this work, nanocrystalline powders of iron-doped zinc oxide ZnO (iron content 3, 5, and 10 at.%) were prepared utilizing co-precipitation method. X-ray diffraction, scanning electron microscopy, and the Mössbauer spectroscopy were used as complementary methods to investigate the structure and hyperfine interactions of the material. It was found that Fe dopant is incorporated into the ZnO würtzite structure. As confirmed by energy-dispersive X-ray spectroscopy the distribution of Fe dopant in the obtained samples is homogeneous up to 5 at.%. For 10 at.% of iron, spinel $ZnFe_2O_4$ phase was registered both by X-ray diffraction and the Mössbauer techniques. Paramagnetic behavior in Fe-doped ZnO was observed in the Mössbauer spectra at room temperature. Hyperfine interactions parameters indicate the presence of Fe^{3+} ions substituting Zn^{2+} ions at tetrahedral sites both in the crystallite interior and near the surface of grains.

DOI: 10.12693/APhysPolA.134.1048

PACS/topics: 61.72.uf, 61.05.cp, 76.80.+y, 31.30.Gs

1. Introduction

Fe-doped ZnO compound belongs to the group of dilute magnetic semiconductors (DMSs). The magnetic properties of these materials depend strongly on the synthesis method, conditions of preparations, etc. They may exhibit room temperature ferromagnetism (RTFM) [1–3], spin-glass behavior [4], superparamagnetic properties [5], and the Curie–Weiss paramagnetism with dominating antiferromagnetic interactions [6]. Due to the poor reproducibility by using different preparation methods or the poor resolutions of the commonly used structural characterization techniques, there are many different interpretation of the origin of magnetism in DMSs. For example, the observed in these compounds RTFM very often is explained by defects; on the other hand, nanosized inclusions of magnetic oxides or metals are usually responsible for the ferromagnetic behavior of the material [1–3].

Metal oxides, like ZnO or TiO_2 doped with transient metals (e.g., Mn, Cr, Fe) present an immense potential for future application in spintronics, spin-polarized light-emitting diodes, non-volatile memory storage or spin valves and transistors [7, 8]. In DMSs, it is possible to control not only the charge of carriers (n- or p-type) as in regular semiconductors, but also intrinsic quantum spin state of electrons. So far, creation of such materials has proven to be challenging and collected data on their properties are inconclusive [9].

Zinc oxide can be observed in two crystalline forms, i.e., hexagonal würtzite (Fig. 1) and cubic zinc blende, the former being most stable at ambient conditions. The bonding in ZnO is ionic (Zn^{2+}–O^{2-}). Hexagonal ZnO belongs to the family of wide band-gap semiconductors, having a band gap of about 3.3 eV at room temperature. Moreover, zinc oxide has piezoelectric and pyroelectric properties [10], hardness of 4.5 on the Mohs scale, high heat capacity and heat conductivity, low thermal expansion and high melting temperature [11].

Interesting issue is the actual oxidation state of iron (Fe^{2+}, Fe^{3+} or the combination of both) in ZnO doped with Fe. Theoretically, both states are possible, i.e., Fe^{2+} in defect-free ZnO or Fe^{2+} and Fe^{3+} in the presence of Zn and O vacancies [12, 13]. Experimentally, it has been reported that Fe atoms occupy the host ZnO lattice in two distinct states Fe^{2+} and Fe^{3+} [14–16], other works pointed to Fe^{3+} ions only [17–19]. Such discrepancy may arise due to the choice of preparation method (e.g., solid-state reaction, mechanosynthesis, wet chemistry methods) as well as due to differences in the preparation conditions of the samples (precursors, reactants,

*corresponding author; e-mail: e.jartych@pollub.pl

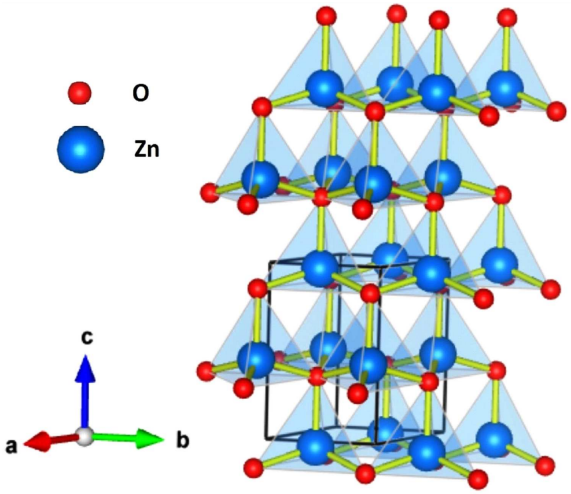

Fig. 1. Hexagonal würtzite structure of ZnO. Elementary cell with parameters $a = b \neq c$ and $\alpha = \beta = 90°$, $\gamma = 120°$ was marked.

reaction/processing temperature, pH, etc.). The main goal of the present studies was to determine the oxidation state of iron and the nearest neighbourhood of Fe ions in the Fe-doped ZnO powders prepared by co-precipitation method. Because the maximum solubility limit of iron in ZnO lattice is about 10 at.% [20], samples with iron content 3, 5, and 10 at.% were selected. The structure and magnetic properties of the obtained material were characterized by means of X-ray diffraction (XRD), scanning electron microscopy (SEM) and the Mössbauer spectroscopy (MS) as complementary methods.

2. Experiment

Fe-doped ZnO powders were prepared by co-precipitation method. Precursors of analytical purity grade $ZnSO_4 \cdot 7H_2O$, $Fe(NO_3)_3 \cdot 9H_2O$ and NaOH were used. The solution of $Fe(NO_3)_3 \cdot 9H_2O$ was used to obtain different molar concentrations of doping, namely 3, 5, and 10 at.% of Fe in ZnO. The estimated aliquot of $Fe(NO_3)_3 \cdot 9H_2O$ was added to a solution of $ZnSO_4 \cdot 7H_2O$. In this base solution, NaOH was added drop wise. During the entire process, magnetic stirring was applied to achieve the precipitate of ZnO compound doped with Fe. Next, this precipitated product was thoroughly washed with de-ionized water to discard residual phases. Drying of precipitate at 100 °C lasted overnight. The dried material was ground and annealed at 400 °C for 5 h. Finally, Fe-doped ZnO powder was ground for further investigations.

XRD studies were carried out at room temperature using PANalytical X-Pert Pro diffractometer with Cu K_α radiation. The phase and structural analyses of the collected XRD patterns were performed with the X'Pert High-Score Plus computer program equipped with the ICDD PDF2 database. Tescan Vega3 LMU scanning electron microscope equipped with X-ray microprobe was used for microstructure observation and elemental analysis. The microscope operated at a 20 kV of acceleration voltage. The homogeneity of the composition was investigated using the energy-dispersive X-ray spectroscopy (EDS). ^{57}Fe Mössbauer spectra were registered at room temperature using POLON spectrometer working in a transmission geometry and constant acceleration mode. A source of ^{57}Co (in a rhodium matrix) with an activity of 50 mCi was used. All values of isomer shift within this paper are related to the α-Fe standard.

3. Results and discussion

The morphology of the obtained powders is presented in SEM images (Fig. 2, top part). Strong agglomeration of the material particles is observed which may be explained by their electrical charging. Co-precipitation method and applied synthesis conditions resulted in a very fine powder samples with a tendency to agglomerate.

As the EDS analysis showed the actual atomic percentage of iron in Fe-doped ZnO powders are 3.0 ± 0.4, 4.6 ± 0.7, and 9.4 ± 0.6 at.%. It may be stated that in the vicinity of the experimental error the concentration of Fe dopant in ZnO is the same as the assumed one. As seen from mapping (Fig. 2, bottom part), distribution of Fe element may be considered as homogeneous in this scale of resolution (similarly Zn and O elements, mapping not presented here).

XRD patterns of all samples shown in Fig. 3 are in good agreement with the würtzite structure of bulk ZnO (PDF2 Card No. 01-079-0207). Small peaks corresponding to spinel phase $ZnFe_2O_4$ were registered in the pattern of ZnO with 10 at.% Fe (indicated by the arrows in Fig. 3). The content of the spinel phase was estimated as 9.5 wt%. It may be noted that signals corresponding to α-Fe, α-Fe_2O_3, γ-Fe_2O_3 or Fe_3O_4 were not detected in any of the samples. A quantitative structural analysis was carried out with the Rietveld refinement method. It was obtained that the a and c lattice parameters do not depend on the iron content and their values are $a = 0.3249(1)$ nm and $c = 0.5206(1)$ nm. This result may be explained by the small differences of ionic radii between iron and zinc. For coordination number 4, iron ions Fe^{2+} and Fe^{3+} have radii 0.63 and 0.49 Å, respectively [21]. The first radius is bigger than that of Zn^{2+} (0.60 Å), whereas that of Fe^{3+} is smaller; therefore, the hexagonal würtzite structure will not strongly change with replacing Zn with Fe ions. Moreover, as reported in [20] for Fe-doped ZnO nanoparticles prepared by sol–gel method, in the Fe concentration range between 1 and 8 at.% lattice parameters a and c practically do not change. Similar results have been obtained for ZnO particles obtained by low-temperature co-precipitation technique [22]. It is worth mentioning that the c/a ratio for our samples of about 1.602 is significantly smaller in comparison to an ideal stoichiometric würtzite structure ($c/a = 1.633$ [23]). This result indicates the presence of oxygen and/or zinc vacancies which are formed to keep charge neutrality.

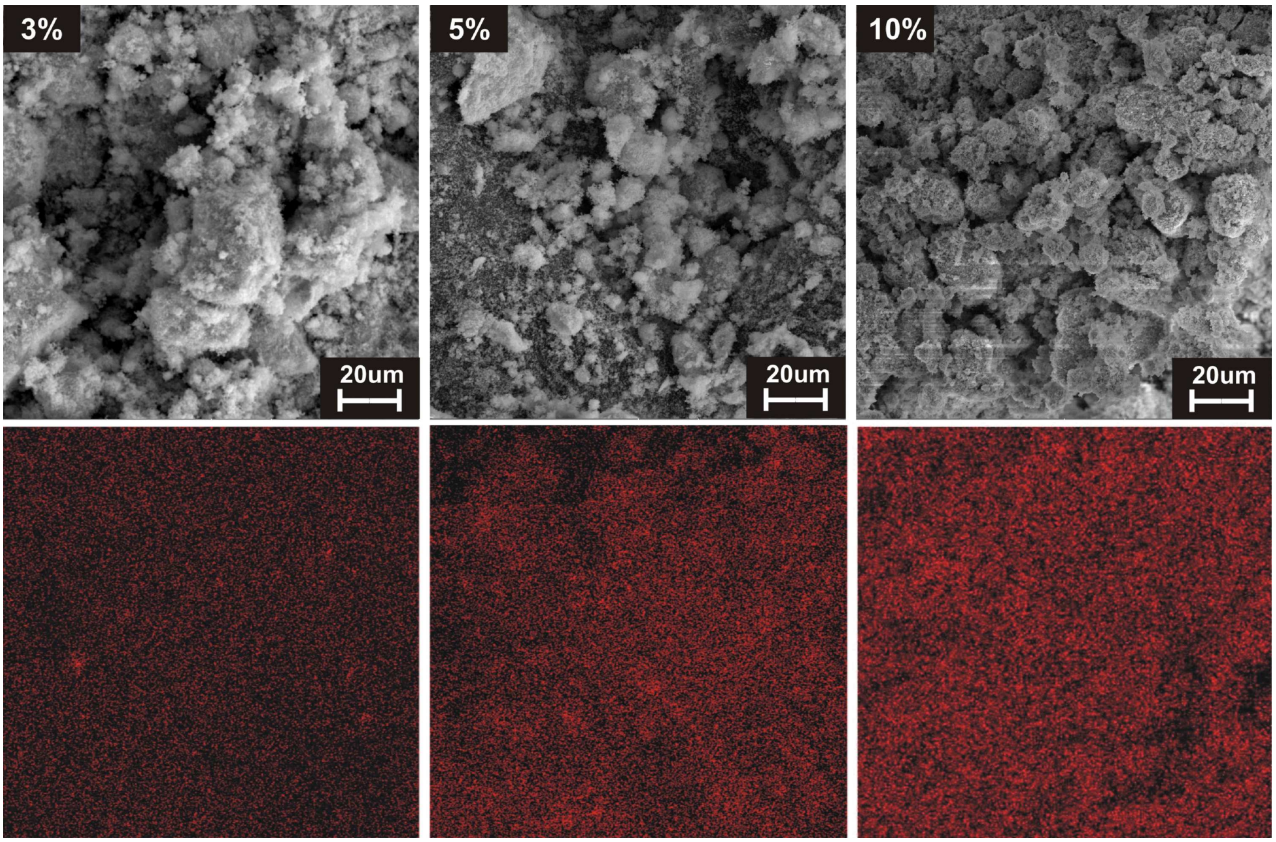

Fig. 2. SEM images of Fe-doped ZnO samples with nominal Fe content 3, 5, and 10 at.% (top part) and mapping of Fe distribution (bottom part).

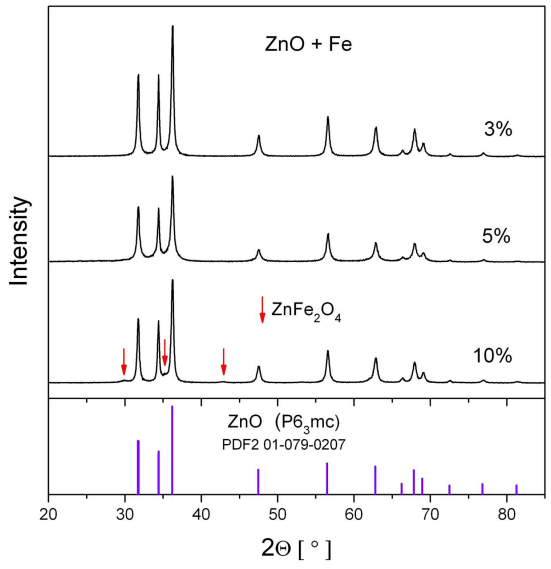

Fig. 3. XRD patterns of Fe-doped ZnO powders with the nominal Fe content 3, 5, and 10 at.%.

With increasing iron content a broadening of the diffraction peaks and decrease in their intensity were observed. The Williamson–Hall method was applied to determine the average crystallite size D and the mean level of lattice strains ε. They are as follows: $D = 120(50)$, 81(17) and 48(20) nm and $\varepsilon = 0.21(2)$, 0.21(2) and 0.09(1) % for Fe dopant content 3, 5, and 10 at.%, respectively. It may be noted that with increasing Fe doping there is a reduction of the average crystallite size. On the other hand, the mean level of lattice strains remains constant for 3 and 5 at.%, while significant reduction of ε for 10 at.% Fe in ZnO may result from the spinel $ZnFe_2O_4$ phase formation. Summarizing structural studies it may be stated that co-precipitation method allowed us to obtain nanocrystalline Fe-doped ZnO powders with a tendency to agglomeration. Up to 5 at.% the distribution of Fe element is rather homogeneous, no iron clusters are seen both in SEM images (in the scale of the method) and XRD patterns. Doping at the level 10 at.% of Fe leads to coexistence of the dominant Fe-doped ZnO phase along with weak spinel phase $ZnFe_2O_4$. The resolution of SEM images does not allow observing single nanocrystals; however, it may be supposed that Fe is incorporated both in ZnO lattice and $ZnFe_2O_4$ structure.

Results of Mössbauer spectroscopy studies are presented in Fig. 4. For all concentrations of Fe dopant spectra have double-line shape. There are no traces of six-line components, thus the existence of α-Fe, α-Fe_2O_3, γ-Fe_2O_3 or Fe_3O_4 phases may be excluded. This result confirms the XRD data. All the Mössbauer spectra were numerically fitted by discrete components, i.e., two or three doublets ($D1$, $D2$, $D3$).

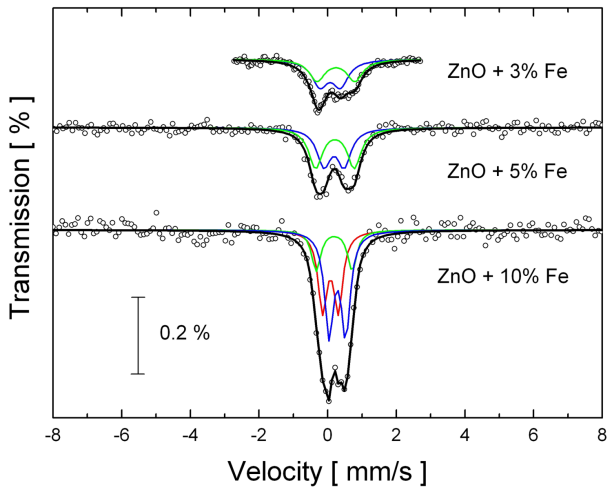

Fig. 4. Room-temperature Mössbauer spectra recorded for Fe-doped ZnO powders with the nominal Fe content 3, 5, and 10 at.%. The components are marked with color lines: blue — for doublet $D1$, green — for doublet $D2$, and red — for doublet $D3$ (spinel $ZnFe_2O_4$).

TABLE I

Hyperfine interactions parameters of Fe-doped ZnO powders derived from room-temperature Mössbauer spectra: δ — isomer shift relative to α-Fe standard, Δ — quadrupole splitting, Γ — half width at half maximum of spectral lines, χ^2 — fitting parameter; uncertainties are given in brackets for the last significant number.

Nominal Fe content [at.%]	δ [mm/s]	Δ [mm/s]	Γ [mm/s]	χ^2	Component
3	0.18(4)	0.59(3)	0.28(1)	0.85	$D1$
	0.34(2)	1.10(2)			$D2$
5	0.28(2)	0.59(2)	0.24(1)	1.04	$D1$
	0.31(1)	1.12(2)			$D2$
10	0.38(1)	0.48(1)			$D1$
	0.29(2)	1.04(1)	0.15(1)	0.86	$D2$
	0.18(3)	0.46(1)			$D3$

The hyperfine interactions parameters of the components are listed in Table I. The values of isomer shift for all doublets are about 0.3 mm/s and suggest that iron ions are in 3+ state. There is no trace of the component with high value of isomer shift ($\approx$ 1 mm/s), thus the existence of Fe^{2+} ions in the samples may be ruled out. The doublets $D1$ and $D2$ fitted in all spectra suggest two different chemical environments of ^{57}Fe nuclear probes. Similar two-doublet model was suggested in the case of the Mössbauer spectra obtained for Fe doped ZnO nanorods [19] or Fe-doped ZnO nanoparticles [20]. In Ref. [19], the authors did not specify the possible surroundings of iron. In Ref. [20], the authors ascribed $D1$ doublet to Fe^{3+} ions in less distorted tetrahedral sites inside the core of ZnO nanoparticles, while $D2$ doublet was assigned to Fe^{3+} ions replacing Zn^{2+} in more distorted tetrahedral sites, i.e., sites close to oxygen and/or zinc vacancies, presumably in the surface region. In the case of our studies, the interpretation reported in [20] is more likely. The values of the isomer shifts and quadrupole splittings of two doublets are very similar to those published in [20]. Thus, we ascribe the first doublet to the Fe^{3+} ions replacing Zn^{2+} in tetrahedral sites inside the ZnO crystallites, while second doublet with higher value of quadrupole splitting may reflect distorted surroundings of ^{57}Fe nuclear probes on the surface of powder particles. The third doublet $D3$ registered in the spectrum for 10 at.% of Fe-doped ZnO sample has the hyperfine interactions parameters which match well with those reported for spinel phase $ZnFe_2O_4$ [24]. This result agrees well with data reported in [20] where spinel phase was observed in the Fe-doped ZnO nanoparticles for dopant content above 5 at.%.

4. Conclusions

The co-precipitation method was successfully used to prepare Fe-doped ZnO powders with fine structure. XRD and MS results proved that Fe dopant is incorporated into the ZnO structure. The analysis of the obtained results suggests that Fe-doped ZnO samples up to 5 at.% Fe are pure and free of both iron oxides and Fe dopant clustering. For higher level of doping (10 at.% Fe), spinel $ZnFe_2O_4$ phase was formed.

Fe ions in ZnO structure do not order magnetically. The values of isomer shifts testify to the third oxidation state of iron. Ions Fe^{3+} substituted Zn^{2+} at tetrahedral sites. Two-doublet model applied in the fitting procedure of the Mössbauer spectra allowed us to attribute first component to the tetrahedral sites of Fe^{3+} ions inside the crystallites and the second one to the more distorted Fe^{3+} sites at the surface of the ZnO powders. The presence of Fe^{3+} ions in ZnO structure inhibits crystallite growth and promotes the formation of oxygen vacancies and/or zinc vacancies.

References

[1] K. Potzger, S. Zhou, *Phys. Status Solidi B* **246**, 1147 (2009).

[2] X. Wu, Z. Wei, L. Zhang, X. Wang, H. Yang, J. Jiang, *J. Nanomater.* **2014**, 792102 (2014).

[3] A.K. Mishra, D. Das, *Mater. Sci. Eng. B* **171**, 5 (2010).

[4] J.E. Ramos, M. Montero-Muñoz, J.A.H. Coaquira, J.E. Rodríguez-Páez, *J. Appl. Phys.* **115**, 17E123 (2014).

[5] J. Neamtu, M. Volmer, *J. Nanomater.* **2014**, 265969 (2014).

[6] S. Kolesnik, B. Dabrowski, J. Mais, *J. Appl. Phys.* **95**, 2582 (2004).

[7] T. Dietl, H. Ohno, F. Matsukura, J. Ciert, D. Ferrand, *Science* **287**, 1019 (2000).

[8] S.B. Ogale, *Adv. Mater.* **22**, 3125 (2010).

[9] J. Barnaś, *Postępy Fizyki* **53D**, 78 (2002).

[10] C.F. Klingshirn, B.K. Meyer, A. Waag, A. Hoffmann, J. Geurts, *Zinc Oxide: From Fundamental Properties towards Novel Applications*, Springer, 2010.

[11] F. Porter, *Zinc Handbook: Properties, Processing, and Use in Design*, CRC Press, 1991.

[12] A. Debernardi, M. Fanciulli, *Appl. Phys. Lett.* **90**, 212510 (2007).

[13] N. Ganguli, I. Dasgupta, B. Sanyal, *Appl. Phys. Lett.* **94**, 192503 (2009).

[14] D. Karmakar, S. Mandal, R. Kadam, P. Paulose, A. Rajarajan, T. Nath, A. Das, I. Dasgupta, G. Das, *Phys. Rev. B* **75**, 144404 (2007).

[15] H. Liu, J. Yang, Y. Zhang, L. Yang, M. Wei, X. Ding, *J. Phys. Condens. Matter* **21**, 145803 (2009).

[16] R. Saleh, S.P. Prakoso, A. Fishli, *J. Magn. Magn. Mater.* **324**, 665 (2012).

[17] M.D. Carvalho, L.P. Ferreira, R.P. Borges, M. Godinho, *J. Solid State Chem.* **185**, 160 (2012).

[18] S. Kumar, Y.J. Kim, B.H. Koo, S.K. Sharma, J.M. Vargas, M. Knobel, S. Gautam, K.H. Chae, D.K. Kim, Y.K. Kim, C.G. Lee, *J. Appl. Phys.* **105**, 07C520 (2009).

[19] M.V. Limaye, S.B. Singh, R. Das, P. Poddar, S.K. Kulkarni, *J. Solid State Chem.* **184**, 391 (2011).

[20] J.J. Beltrán, C.A. Barrero, A. Punnoose, *Phys. Chem. Chem. Phys.* **17**, 15284 (2015).

[21] *CRC Handbook of Chemistry and Physics*, Ed. D.R. Lide, 87th ed., CRC Press, 2006.

[22] T.A. Abdel-Baset, Y.-W. Fang, B. Anis, C.-G. Duan, M. Abdel-Hafiez, *Nanoscale Res. Lett.* **11**, 115 (2016).

[23] H. Morkoc, U. Ozgu, *Zinc Oxide: Fundamentals, Materials and Device Technology*, Wiley-VCH, Weinheim 2009.

[24] F. Li, H. Wang, L. Wang, J. Wang, *J. Magn. Magn. Mater.* **309**, 295 (2007).